PROCEEDINGS OF SCIENCE

Energy-dependent imaging properties of the Medipix2 X-ray-detector

Thilo Michel[1]
Physikalisches Institut Universität Erlangen-Nürnberg
Erwin-Rommel-Str. 1, 91058 Erlangen, Germany
E-mail: Thilo.Michel@physik.uni-erlangen.de

The first part of this contribution covers simulation studies and measurements of imaging properties of the Medipix2 detector. Position resolving properties of the Medipix-detectors described by the so-called modulation transfer function (MTF) in dependence on the discriminator threshold and on primary energy will be discussed. The MTF shows a significant drop at low spatial frequencies due to the emission and detection of fluorescence photons from the backside, e.g. the bump-bonds and the silver containing glue between the ASIC and the chipboard. The second part is focused on the energy resolving properties of the Medipix detectors and their exploitation in X-ray imaging. Simulation results of the monoenergetic response functions, taking diffusion in the sensor layer and backscattering from the chipboard into account, are in good agreement with measurements. Two methods have been developed to calculate the impinging energy spectrum with the measured energy deposition spectrum. These methods allow the determination of the material composition of an irradiated object. The successive application of the pseudo-inverse of an attenuation coefficient matrix of known materials on the reconstructed transmitted spectrum in each pixel gives quantitative values of the material concentration in the object. The determination of material concentrations of a phantom comprising several materials is shown in a measurement. The Medipix3 with its so-called color mode will offer excellent possibilities to use this method.

The 16th International Workshop on Vertex Detectors
Lake Placid, NY, USA
23 – 28 September 2007

[1] Speaker

PoS(Vertex 2007)044

1. The Medipix2 detector and the detection principle of x-rays

The Medipix2 detector [1] is a hybrid photon counting semiconductor pixel detector, which has been developed by an international collaboration [2]. The ASIC has been designed at CERN. Due to the hybrid design the ASIC can be combined with different sensor materials like silicon, GaAs or CdTe. In this contribution we restrict our considerations to a standard Medipix assembliy bump-bonded to a silicon sensor with a thickness of 300 µm, biased with 150 V. The sensor layer with its matrix of 256 x 256 pixel electrodes is bump-bonded to the Medipix2-ASIC via bump-bonds of a lead-tin-alloy. The Medipix detector was first designed for applications in x-ray imaging where energies range from about 5 keV up to 150 keV. An impinging x-ray photon may interact in the sensor material via Compton- or photoelectric effect. An electron is released from the reacting atom and travels through the sensor material. It releases electron-hole-pairs along its track. In this energy range the average scattering angle of single collisions of the compton- or photoelectron are large so that the electron quickly loses information about its initial direction of ejection. The size of the distribution of free charge carriers that is released along the electrons track is in the order of several microns. Multiple scattering leads to a rather curled track and an approximately spherical charge carrier distribution. Due to the track length in the order of several microns, which is not negligible compared to the pixel pitch of 55 µm, a significant part of the electrons reaches the sensitive sensor volume of a neighboring pixel. This results in production of electron-hole-pairs in the detection regime of the neighboring pixel. Additionally the compton-scattered photon may interact in the sensor layer again and trigger a second pixel. Figure 1 is an illustration of the detection processes. The production of fluorescence photons also can cause triggering of additional pixels, if the energy of the fluorescence photons is large enough. The energies of the K_α lines of silicon are only about 1.7 and 1.8 keV which is below the minimum discriminator threshold. If GaAs or CdTe are used, the detection of fluorescence photons has an impact on the position resolution of the detector. The distribution of electrons is separated immediately from the holes by the applied electrical field. The Medipix2-ASIC can be operated in electrons- or in holes-collection mode. The standard combination with the silicon sensor is operated in holes-collection mode. In this case the holes are drifted towards the pixel electrodes. During its drift, the charge cloud diffuses and therefore extends its dimensions. For a point-like initial charge the radius of the distribution can be approximated by the standard-deviation of a Gaussian [5].

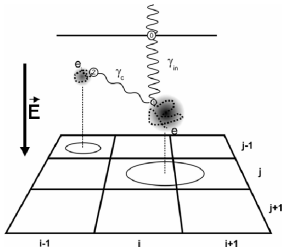

Figure 1: Illustration of detection processes which are described in more detail in [3][4]

The current signal that is induced in the pixel electrodes by the moving charges is transferred into the input of the pixel electronics via the bump-bond. In the analog part of the pixel electronics the current signal is amplified, integrated and converted to a voltage signal which is proportional to the collected charge. This signal is compared to two adjustable, global discriminator thresholds. The two discriminators can be operated in the window- or in the single-threshold-mode. In the window mode a digital signal is generated if the amount of collected charge and therefore the energy deposition in the pixel is between both discriminator thresholds. In the single-threshold mode a digital signal is generated if the energy deposition is larger than the threshold. In our investigations we used the single threshold mode. Three so-called threshold adjustment bits can be set for each pixel separately so that slight variations of the energetic level of the thresholds among the pixels are corrected. The minimum threshold that can be used in x-ray imaging is about 3 keV. Upon detection of the x-ray photon a 14-bit counter, realized as pseudo-random-counter, is incremented. Further counting of x-ray photons is inhibited during read-out by a global shutter signal. The pseudo-random-counters then act as shift registers and their content is transferred to the read-out area of the ASIC. The counter values, which are the number of detected events in the pixels, are transferred to the periphery either via serial LVDS or via a parallel 32-bit-CMOS-bus. Readout of the whole matrix is possible serially in about 9 msec and in about 265 μsec using the parallel readout. The most important advantages of the Medipix2 detector for applications in x-ray imaging compared to standard flat panel detectors are the existence of an energy equivalent threshold, giving access to energy information of individual photons and producing noise-free dark images which is important for good low-contrast resolution. Imaging of low energetic x-ray photons can be performed even at very low flux.

2. Imaging properties of the Medipix2

2.1 Position resolution

The position resolving properties of an imaging detector in one dimension can be characterized by the Modulation-Transfer-function (MTF). The MTF is defined as

$$MTF(f) = \frac{C_{out}(f)}{C_{in}(f)}$$

where f is the spatial frequency, $C_{in}(f)$ is the contrast of the signal in the impinging radiation field and $C_{out}(f)$ is the contrast in the image. The contrast is defined as:

$$C = \frac{I_{\max} - I_{\min}}{I_{\max} + I_{\min}}$$

where I is the intensity of the signal. It can be shown that the MTF can be written as the normalized Fourier-transform of the line-spread-function (lsf), which is the response of the detector to a line-shaped input signal:

$$MTF(f) = \frac{\left|[FT(lsf)](f)\right|}{[FT(lsf)](0)}$$

We measured the MTF of the Medipix2 detector by positioning a tungsten plate in parallel to the sensor layer with an inclination angle of about 2 degrees between the edge of the tungsten plate to the columns of the pixel matrix and by irradiating the setup with x-rays produced in an x-ray tube at acceleration voltages between 40 kV and 140 kV for different discriminator threshold settings [7]. We used the data acquisition software Pixelman [8]. We define the x-axis to be the direction of the rows in the matrix. After calculation of the distance x between the edge position to the center of the pixel that is partly covered and after reorganization of the data which is necessary due to the over sampling of the pixel area we can project the intensities to the x-axis. The result of this projection is the so-called edge-spread-function esf(x). Figure 2 (left hand side) shows the measured edge-spread-functions for irradiation with 90 kV acceleration voltage for discriminator thresholds at 5.75 keV (black), 15 keV (red), 20.1 keV (green) and 45.15 keV (blue). It can be seen that the steepness of the edge rises with increasing threshold energy due to the reduction of the amount of events which had suffered charge sharing in the sensor layer. Figure 2 (right hand side) shows the derivatives of the edge-spread-functions, which are the line spread functions to be used to calculate the modulation transfer functions.

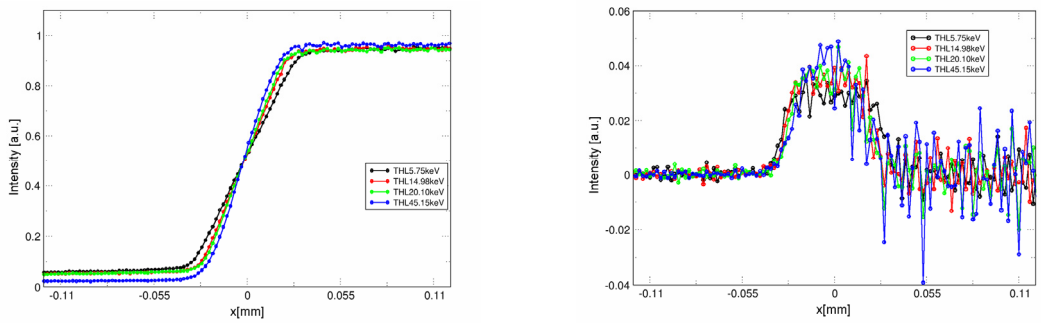

Figure 2: Measured edge-spread-functions (esf) and corresponding line-spread-functions (lsf) for several discriminator thresholds

Figure 3 shows the measured compared to the simulated modulation transfer function for irradiation with an x-ray spectrum at 90 kV tube voltage and a discriminator threshold of 6 keV as a function of spatial frequency given in line-pairs per mm. We want to point out that no correction like smoothing or offset removal has been applied to our data. In certain standards some processing is allowed during calculation of the modulation transfer function. Therefore care has to be taken if the modulation transfer function that we show here is compared to the modulation transfer function of other detectors. It can be seen that our simulation with the Monte-Carlo program ROSI [6] reproduces the measured data very well. The modulation transfer function reaches its zero point at a frequency of about 15.8 line pairs per mm, corresponding to an effective pixel width of about 63 µm. Figure 3 also shows the modulation transfer function of an ideal pixel detector with a pixel pitch of 55 µm. The modulation transfer function of an ideal detector, which is not suffering from charge sharing and has a homogeneous response over the pixel area, is given by the Fourier-transform of the Box-function, which is a sinc-function. It is clearly visible (red box in figure 3) that the modulation transfer function of the Medipix2 detector at low spatial frequencies is lower than the MTF of the ideal detector.

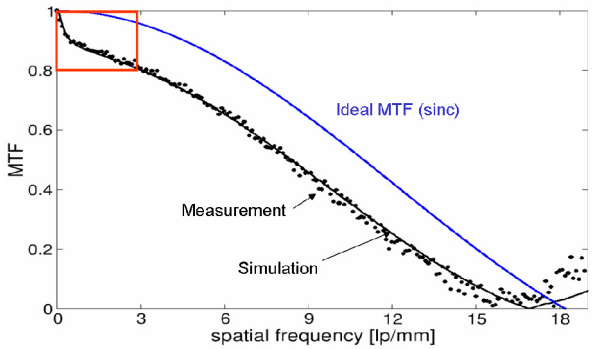

Figure 3: Measured and simulated modulation transfer functions for a 90 kV x-ray spectrum with 6 keV discriminator threshold together with the MTF of an ideal detector with 55 µm pixel pitch

This so-called low-frequency-drop of the MTF is due to the detection of fluorescence photons which are generated by photons which transmitted the sensor layer and are absorbed in the bump-bonds or in the silver containing, heat conducting glue which sticks the ASIC to the printed circuit board. The emission of fluorescence photons is an isotropic process and therefore leads to additional detection of the fluorescence photons far away from the original point of transit through the sensor. This long range effect thus has an impact on low spatial frequencies and degrades the MTF. The relevant energies of the fluorescence photons are approximately 22.1 and 25 keV for production in silver and 25.2 and 28.5 keV for generation in the tin of the bump-bonds. The thickness of the silver containing glue varies among the assemblies. Figure 4 shows simulation results of the modulation transfer function for several thicknesses of the silver containing glue in comparison with the measured functions. One can see that the measured modulation transfer function is represented very well with our simulations if we assume a thickness of about 30 µm for the glue layer. If the glue layer is ignored in the simulation, a strong discrepancy with the experiment is visible.

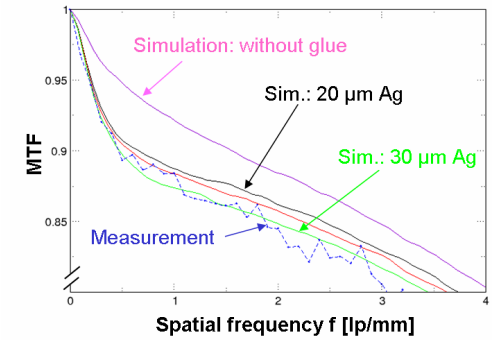

Figure 4: The measured compared to simulated modulation transfer function for different thicknesses of the glue layer

Figure 5 shows pixel profiles measured with the edge method for an acceleration voltage of 90 kV of the tungsten tube for discriminator thresholds at 6, 15 and 45 keV.

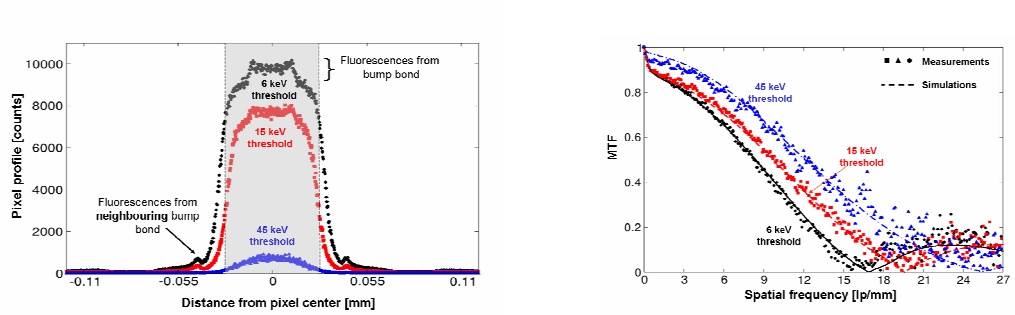

Figure 5: Measured pixel profiles (left hand side) and corresponding modulation transfer functions compared to simulation results (right hand side) at different discriminator thresholds

The width of the effective pixel profile decreases with increasing threshold energy as it is expected because of the suppression of the influence of charge sharing effects. At 6 keV threshold energy the FWHM of the effective pixel profile is larger than the pixel pitch, equal to the pixel pitch at about 15 keV threshold energy and smaller than the pixel pitch at 45 keV threshold energy. The structure on the top of the effective pixel profile at low discriminator thresholds is due to the generation of fluorescence photons in the bump bond of the pixel followed by their detection in the pixel which is geometrically favored due to the fact that the bump bond is adjacent to the pixel sensitive volume. The effect of detection of fluorescence photons from the bump bond of the neighboring pixel is also visible. The structures vanish, if the threshold energy is higher than the energy of the fluorescence photons. For 45 keV threshold energy, which is half of the maximum primary energy in the spectrum, only events which have deposited the major part of their energy in the pixel are detected thus leading to reduced detection efficiency at the edges of the pixel and thus reducing its effective width. Figure 5 also shows the corresponding modulation transfer functions calculated with the measured pixel profiles in comparison to simulation results. As can be seen, the first zero point increases with increasing threshold energy due to reduction of the charge sharing effects. The low frequency drop vanishes for threshold energies above the energy of K_α fluorescence photons of silver and tin. The gain in the contrast transfer for the step from 6 keV to 15 keV is due to the suppression of charge sharing effects. Simulations and measurements agree very well. This shows that the modeling of the charge carrier production and their motion in our simulation code is accurate.

2.2 The detective quantum efficiency

Charge sharing causes correlated counting of different, especially neighboring, pixels. Assuming a radiation source with poissonian intensity variations the number of counts in each pixel varies according to Poisson statistics. The sum of the counts in several pixels is varying stronger due to the counting correlation. This has an impact on the image noise and therefore on the imaging quality of the detector. The Detective Quantum Efficiency (DQE) is a measure for the information transfer quality from the impinging radiation pattern to the image. The DQE is defined as the squared ratio of the outgoing to the incoming signal to noise ratio of an imaging

system. Introducing the event multiplicity and applying error propagation it can be shown [9] that the zero spatial frequency DQE(0) can be expressed in terms of the average event multiplicity <m>, the average squared event multiplicity <m^2> and the detection efficiency ε:

$$DQE(0) = \frac{SNR_{out}^{\ 2}}{SNR_{in}^{\ 2}} = \frac{\langle m \rangle^2}{\langle m^2 \rangle} \varepsilon$$

Figure 6 (left hand side) shows simulation results of quantities in this formula for the zero spatial frequency DQE in dependence on discriminator threshold irradiating the Medipix2 detector with a standard x-ray spectrum of a molybdenum anode at 40 kV acceleration voltage. It can be seen that the information transfer efficiency of the detector is reduced by up to 15 % due to the multiplicity depending factor in the formula. The DQE(0) shows a plateau at low discriminator threshold were losses in the efficiency with increasing discriminator threshold are compensated by noise reduction through reduction of multiple counting. The discriminator threshold should be adjusted in this region. Figure 6 (right hand side) shows the average (squared) multiplicity as a function of discriminator threshold for monoenergetic irradiation at 100 keV. As expected, the multiplicities are higher for thresholds below the Compton edge at about 28 keV.

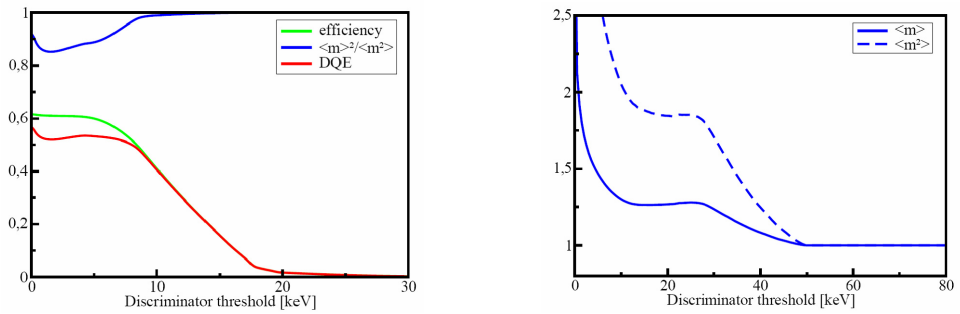

Figure 6: Quantities affecting the DQE(0) in dependence on threshold energy for irradiation with a 40 kV molybdenum spectrum (left) and 100 keV monoenergetic irradiation (right)

2.3 Response function

The response function of a pixelated photon counting detector for a certain primary energy, which is the probability for detecting a photon as a function of its energy deposition, depends for example on the pixel pitch, the sensor material, the bias voltage, and the sensor thickness. The measured and simulated response functions of the Medipix detector with 300 µm silicon sensor biased with 150 V for a primary energy of 59.3 keV are shown in figure 7. The measurement was carried out by performing a threshold scan during irradiation with x-ray photons from a monochromator setup using Bragg reflexion from a silicon crystal illuminated with radiation from an x-ray tube. At this energy the photopeak is still visible. Charge sharing and Compton scattered electrons cause the tail down to lower energy deposition values. The

structure between 20 and 26 keV is caused by the detection of K_α fluorescence photons from tin in the bump bonds and the silver in the glue. Our simulations reproduce the measured response function very well.

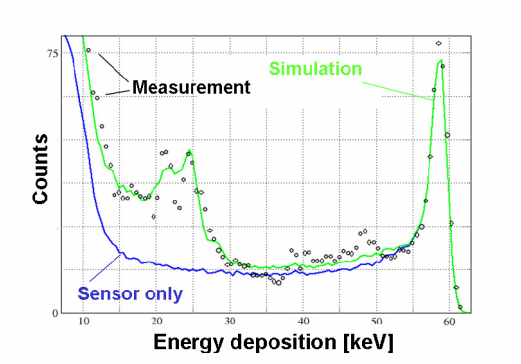

Figure 7: Measured and simulated energy deposition spectrum at 59.3 keV primary energy

3. Applications of the energy resolving properties

3.1 Reconstruction of incident x-ray spectra

The broad response function of the Medipix2 detector and the efficiency of silicon, which is decreasing strongly with energy, result in a spectrum of deposited energies which looks very different to the impinging spectrum. A calculation of the impinging spectrum is possible by means of deconvolution methods. The advantage of the Medipix2 detector for measurements of x-ray spectra is that the spectrum can be determined at very high flux due to the small pixel size. This is typically the case with x-ray tubes. In order to reconstruct the impinging spectrum we simulated the monoenergetic response functions in primary energy steps of 0.5 keV from 5 to 150 keV. We measured the energy deposition spectrum by performing a threshold scan while irradiating the Medipix2 with x-rays from a tube. Calculation of the derivative of the number of counts as a function of threshold energy gives the energy deposition spectrum. Thresholds were calibrated with x-rays from radioactive sources. The measured energy deposition spectrum can be written as the superposition of the monoenergetic response functions multiplied with the number of impinging photons for each primary energy:

$$M(E_i') = \sum_{j=1}^{N} R(E_i', E_j) \cdot S(E_j)$$

Here, E' denotes energy deposition, E stands for primary energy, R is the response function of the detector to monoenergetic radiation and S is the unknown impinging spectrum. $R(E_i', E_j)$ is the probability that an impinging photon of energy E_j causes an energy deposition of E_i'.

This equation can be written in compact vector notation:

$$\vec{M} = R \cdot \vec{S}$$

We used two methods in order to reconstruct the impinging spectrum: the matrix inversion method and the spectrum stripping method.

In the matrix inversion method we applied the pseudo-inverse of the matrix R (containing the monoenergetic response functions) to the measured energy deposition spectrum. The result is a best estimation of the impinging spectrum in a maximum-likelihood-sense:

$$\vec{S} = (R^T R)^{-1} R^T \cdot \vec{M}$$

Figure 8 (left hand side) shows the reconstructed impinging spectrum calculated with measured data in comparison to the theoretically impinging spectrum of a tungsten x-ray tube at 120 kV acceleration voltage. Excellent agreement is clearly visible. Even the fluorescence lines of tungsten are reconstructed with good energy resolution.

The spectrum-stripping-method is a successive method. In the first step we assume that the events occurring at the maximum measured energy deposition are caused by photons of this energy. We scale the corresponding monoenergetic response function, which was defined in chapter 2.3, so that the measured number of counts in the high-energetic energy deposition bin is equal to the number of counts in the maximum of the scaled response function. Then we subtract the complete scaled response function from the measured energy deposition spectrum. We move to the next smaller energy deposition bin and scale the corresponding response function so that we can reduce the remaining measured number of counts in the energy deposition spectrum also to zero. This process is performed until the energy deposition spectrum is finally completely reduced to zero. The scaling factors that are used in the steps give the impinging spectrum. Figure 8 (right hand side) shows the reconstructed impinging spectrum from measured data in comparison to the theoretically impinging spectrum of a tungsten x-ray tube at 80 kV acceleration voltage. It is visible that also this successive reconstruction method works very well.

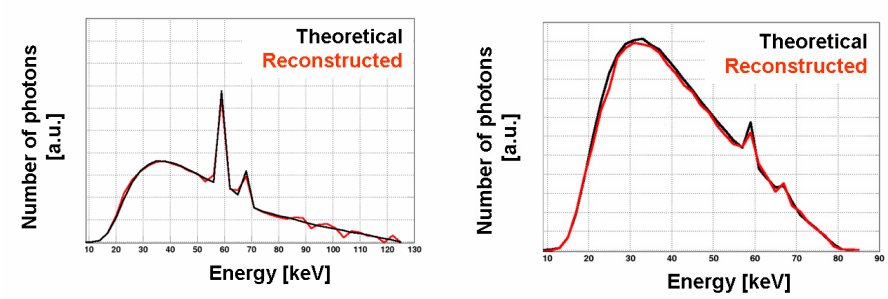

Figure 8: Results of the calculated impinging spectrum compared to expected spectra using the matrix inversion method (left hand side) and spectrum-stripping-method (right hand side)

3.2 The method of material decomposition

With the ability to calculate the spectrum one is able to determine the spectrum that has transmitted an object positioned between x-ray tube and detector. Due to the fact that each pixel of the Medipix2 has its own discriminator, this can be done pixel-wise giving an image of transmitted spectra. If the spectrum incident on the object is known, information on the material composition of the irradiated object can be obtained because each material modifies the radiation field in a specific manner, which is described in the following formula for an object comprising m different materials:

$$t(E_i) = -\ln T(E_i) = -\ln \frac{N(E_i)}{N_o(E_i)} = \sum_{j=1}^{m} \left[\frac{\mu(E_i)}{\rho} \right]_j \cdot \quad p_j$$

Here, E denotes the primary energy, N(E) the number of transmitted photons with energy E, N_0 the number of impinging photons, $(\mu/\rho)_j$ the mass attenuation coefficient of material j, and p_j the areal density of material j projected along the path of the x-rays. Our aim is to determine the areal densities of each material in front of each pixel. Assuming to have carried out a pixel-wise measurement of the transmitted spectrum (threshold scan plus spectrum deconvolution as described above) a set of coupled equations can be written in vector notation with the matrix M having the mass attenuation coefficients of the materials as functions of energy as its components:

$$\vec{t} = M \cdot \vec{p}$$

This set can be solved pixel-wise by applying the pseudo-inverse of the materials matrix to the logarithmized transmitivities t calculated with the reconstructed transmitted spectra:

$$\vec{p} = \left[(M^T M)^{-1} M^T \right] \cdot \vec{t}$$

Due to the fact that beam-hardening (which is depending on the material composition of the object) affects the transmitted spectrum, our method has to be carried out iteratively. To do this, the average mass attenuation coefficients in the energy bins in the materials matrix are recalculated several times with the solutions of the set of equations. It has to be pointed out that our method gives quantitative values of the areal densities of the materials in the object. The method works best if materials with K-edges in the used energy range are present in the object.

3.3 Experimental test of the material decomposition

First tests with a phantom consisting of a block of Polymethylmethacrylat (PMMA) with a hole filled with water-iodine-solution and an aluminum plate have been performed [10] with a 50 kV tube spectrum. Figure 9 shows a picture of the phantom and a photon counting image.

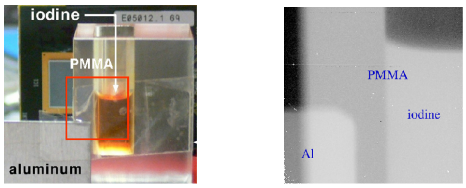

Figure 9: Picture of the phantom and a projective photon counting image

The areas behind different materials show contrast, but no material information can be gained from the photon counting image. After having carried out a threshold scan during irradiation, followed by the pixel-wise calculation of the transmitted spectrum followed by the application of the material decomposition described above we were able to extract the images in figure 10 of the projected areal densities of iodine, PMMA and aluminum. The green arrows indicate the theoretical value of the areal density. It can be seen, that the iodine image only shows a signal in the area where iodine is present. The expected areal density of iodine in the phantom (p = 0.027 g/cm^2) is measured correctly. The aluminum plate is only visible because of an increased noise. There is no average signal in the aluminum region of interest in the iodine image. No PMMA is visible in the iodine image.

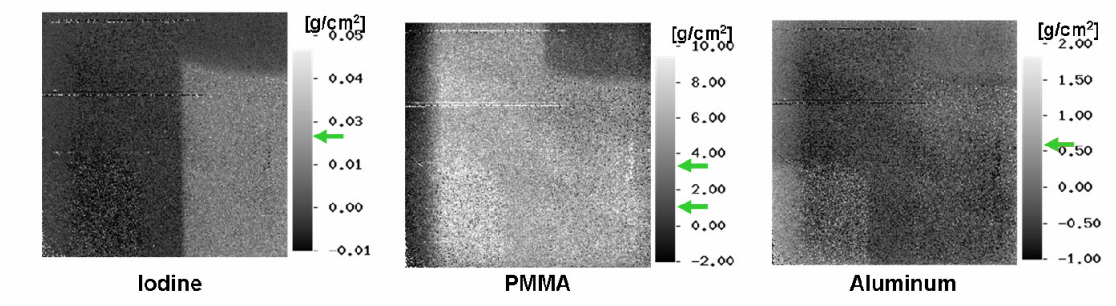

Figure 10: Reconstructed material images

In the PMMA image one can distinguish between the two regions (middle part and upper right hand side part) where different thicknesses of PMMA are in the x-ray path. Again, the areal densities have their correct values of 1.2 and 3.6 g/cm^2. In the aluminum image the aluminum plate is visible with a non-zero contrast to the rest of the image. In the region where no additional PMMA is behind the aluminum, the areal density is determined with the correct value of 0.54 g/cm2. There are still some structures of PMMA and water visible in the aluminum image which are due to the similar behavior of aluminum, PMMA and water, and due to the influence of scattering. This shows that the material decomposition method in principle works. We are currently working on improving our reconstruction quality with finer binning of the energy deposition and reconstruction energy intervals. This method may have important applications in medical x-ray imaging especially when contrast agents of iodine or gadolinium are used. This may reduce the necessary dose to the patient. The method may also be used in

homeland security applications like luggage screening in order to identify materials and their concentration which are present in the examined object.

3.4 Outlook: the Medipix3 with its charge summing mode

The Medipix3 detector is currently in its design phase. The charge summing mode is the most important feature of the novel AISC for applications of the material decomposition. In the charge summing mode, the analog circuitry in each pixel (again with a pitch of 55 µm) generates four copies of the charge input signal which are proportional to the input charge. The four copies are sent to common nodes of each 2 by 2 pixel neighborhood. There the current signals are added, the sum is compared to a threshold and the event is counted.

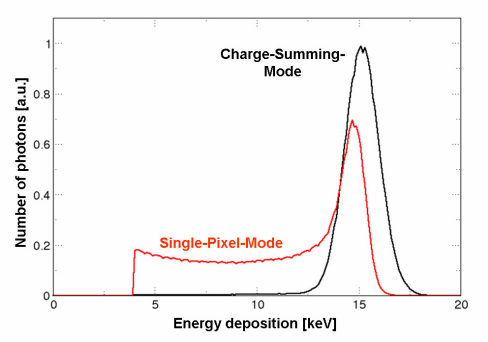

Figure 11: Simulated response function in single pixel mode (Medipix2) and in charge summing mode (Medipix3) for irradiation with 15 keV photons

Figure 11 shows simulation results on the response function of the Medipix3 in comparison to the energy response of the Medipix2 at 15 keV using noise values which were derived from measurements with the Medipix3 test-chip [11]. It can be seen that in the charge summing mode almost all of the events are detected with an energy deposition close to the primary energy. Reconstruction of impinging spectra and therefore material decomposition will profit from this improved response function. Additionally the Medipix3 offers the possibility – if bump-bonded to a sensor chip with 110 µm pixel pitch – to use the 2 x 4 thresholds in the 4 subjacent nodes to accumulate events in 8 energy bins simultaneously. Therefore it is possible to apply material decomposition to images taken with only one x-ray shot. In contrast to the Medipix2 no threshold scan will be necessary with the Medipix3. This reduces the dose delivered to the object. The possible accuracy of the calculation of material density images using 8 energy deposition bins has to be investigated. A detailed description of the Medipix3 functionalities can be found in [11].

Acknowledgement

This work was carried out within the Medipix collaboration. The author would like to thank the whole collaboration.

References

[1] X. Llopart et al, *Medipix2: a 64-k Pixel Readout Chip With 55-mm Square Elements Working in Single Photon Counting Mode*, IEEE Trans. Nucl. Sci., Vol. 49, No. 5, 2002

[2] http://medipix.web.cern.ch/MEDIPIX/

[3] G. Anton et al., *Imaging theory for X-ray pixel detectors*, Nucl. Instr. Meth. A563 (2006) 116-123

[4] M. Mitschke et al, *Simulation of signal generation processes in semiconductor sensor layers for Medipix1 and 2,* Nucl. Instr. Meth. A531 (2004) 62-67

[5] H.G. Spieler et al, *Assessment of present and future large-scale semiconductor detector systems,* IEEE Trans. Nucl. Sci., Vol. NS-32, No. 1, February 1985

[6] J. Giersch et al, *ROSI—an object-oriented and parallel-computing Monte Carlo simulation for X-ray imaging*, Nucl. Instr. Meth. A509 (2003) 151-156

[7] P. Bartl et al, *Measurement and detailed simulation of the Modulation Transfer Function of the Medipix2*, in proceedings of the 9th IWORID, to be published in Nucl. Instr. Meth. A

[8] T. Holy et al, *Data Acquisition and Processing Software Package for Medipix-2 Device,* Nucl. Instr. Meth. A563 (2006), Issue 1, 254-258

[9] T. Michel et al, *A fundamental method to determine the signal-to-noise ratio (SNR) and detective quantum efficiency (DQE) for a photon counting pixel detector*, Nucl. Instr. Meth. A568 (2006) 799-802

[10] M. Firsching et al, *Material Resolving X-ray imaging using Spectrum Reconstruction with the Medipix2*, in proceedings of the 9th IWORID, to be published in Nucl. Instr. Meth. A

[11] R. Ballabriga et al, *The Medipix3 Prototype, a Pixel Readout Chip Working in Single Photon Counting Mode with Improved Spectrometric Performance*, IEEE Trans. Nucl. Sci., Vol. 54, No. 5, October 2007